Effect of NaOH concentration as activator on calcined eggshell and its application for yeast microbial fuel cell

by Satrio Kuntolaksono

Submission date: 01-Mar-2023 03:24PM (UTC+0500)
Submission ID: 2026071057
File name: MarcelJoeliSatrioAchmad_RIM_28_January_2023.pdf (4.77M)
Word count: 9102
Character count: 47438

Bioresource Technology Reports 21 (2023) 101347

Contents lists available at ScienceDirect

Bioresource Technology Reports

journal homepage: www.sciencedirect.com/journal/bioresource-technology-reports

Effect of NaOH concentration as activator on calcined eggshell and its application for yeast microbial fuel cell

Marcelinus Christwardana[a,b,*], J. Joelianingsih[c], Satrio Kuntolaksono[c], Achmad Yanuar Maulana[d,e]

[a] Department of Chemistry, Diponegoro University, Jl. Prof. Sudarto SH, Tembalang, Semarang, Central Java 50275, Indonesia
[b] Master Program of Energy, Diponegoro University, Jl. Imam Bardjo SH, Pleburan, Semarang, Central Java 50241, Indonesia
[c] Department of Chemical Engineering, Institut Teknologi Indonesia, Jl. Raya Puspiptek Serpong, South Tangerang 15014, Indonesia
[d] Department of Chemistry, Dong-A University, Busan, 49315, South Korea
[e] Asosiasi Peneliti Indonesia di Korea (APIK), Seoul 07342, South Korea

ARTICLE INFO

Keywords:
Waste utilization
Advanced material
Green material
Bioenergy
Bioelectricity

ABSTRACT

Eggshells may be utilized as an advanced material. Yeast microbial fuel cells may benefit with calcined eggshell at carbon felt anodes. Stability issues and poor power density prohibit its wider usage. We determined the eggshell-to-NaOH ratio for calcined eggshell anode material. Calcined eggshell with a 1:4 eggshell-NaOH ratio had a high maximum power density (31 $mW.m^{-2}$) and voltage stability of 45 mV after 30 days incubation. The addition of NaOH activator may also increase crystal size and crystallinity to 145 nm and 43.92 %, respectively, which may accelerate electron transport as evidenced by a decrease in the energy band gap from 5.6 to 5.2 eV, as determined by DFT analysis. The addition of NaOH activator during incubation increased the surface area to 181.2 $m^2.g^{-1}$, improving the anode's potential to host yeast biofilms. Calcined eggshell with a 1:4 eggshell-NaOH ratio is a good anode for yeast microbial fuel cells.

1. Introduction

Fossil fuels have powered the country's industrialization and socio-economic development during the past century. It cannot, however, sustain the global economy continuously (Mudakkar et al., 2013). Even though oil will not run out for at least another hundred years, it is predicted to run out in the next ten to twenty years as demand exceeds supply. In the next decades, the cost and quantity of energy we use will dictate our economy and way of life (Logan, 2008). Population expansion and growing energy consumption will lead to the depletion of fossil fuels and a rise in CO_2 emissions, which might create additional environmental and health problems on a worldwide scale (Peera et al., 2021; Apollon et al., 2022a, 2022b). In addition, increased industrialization and the need for new technology have led to different forms of environmental degradation, particularly water pollution (Peera et al., 2021). Therefore, it is essential to develop sustainable and renewable energy sources.

Microbial Fuel Cells (MFCs) are an eco-friendly technology with the potential to reduce the effects of organic waste-caused environmental pollution (Sravan et al., 2021). MFCs are fuel cells that use active microorganisms as biocatalysts in the anode's anaerobic compartment to produce power (Rahimnejad et al., 2015). During metabolic activities, microorganisms get energy from organic materials (Liu et al., 2019). Microorganisms digest organic materials by transforming it into protons and electron ions. Depending on the potential difference between these ions, they may produce electricity (Kim et al., 2020).

Due to the high cost of electrode materials and poor electrode performance, electron transmission from the microbe to the electrode is sluggish in MFCs. Metal-based materials are the most common raw materials utilized in the production of electrodes. However, the high cost of metallic components and the lack of MFCs' long-term stability severely limit their commercial use (Gong et al., 2020). Despite being a promising technology, the development of MFCs faces several obstacles due to their lower power output compared to conventional fuel cells. Current MFCs are difficult to scale up or commercialize because to the high cost of materials and crucial components (Offei et al., 2016). In the development of MFCs technology, cost, and performance are crucial issues. The failure to enhance extracellular electron transfer activity and the absence of biofilm development as a consequence of poor microbial adhesion to the anode surface would further limit the performance of

* Corresponding author at: Department of Chemistry, Diponegoro University, Jl. Prof. Sudarto SH, Tembalang, Semarang, Central Java 50275, Indonesia.
E-mail address: marcelinus@lecturer.undip.ac.id (M. Christwardana).

https://doi.org/10.1016/j.biteb.2023.101347
Received 24 October 2022; Received in revised form 15 January 2023; Accepted 23 January 2023
Available online 28 January 2023

MFCs (Christwardana et al., 2021). As a consequence, researchers are concentrating on creating low-cost electrode materials with great stability in order to solve this problem.

One approach for solving for the drawbacks of MFCs is to modify the electrodes into sustainable materials by using waste as anode material in order to reduce their high prices and aid in the treatment of environmental waste (Balasubramanian et al., 2020). Due to their high conductivity, specific surface area, biocompatibility, chemical stability, and low cost, carbon materials such as graphite rods, graphite fiber brushes, carbon cloth, carbon paper, and carbon felt are often used as anodes in MFCs (Mustakeem, 2015). However, these carbon-based electrodes have certain drawbacks, such as graphite rods that are difficult to expand in surface area, graphite fiber brushes that are prone to clogging, relatively costly carbon cloth, brittle carbon paper, and carbon felts with high resistance (Mustakeem, 2015).

The anode is the MFC's most crucial performance component. Biofilms are formed by microorganisms cultivated in the anode chamber to generate energy, which has been essential for the advancement of MFC technology (Davis and Yarbrough, 1962). In addition, the anode acts as a platform for electrochemically active bacteria capable of capturing electrons through an exoelectrogenic process. In contrast, the anode material may influence the capital expenses connected with the commercialization of MFCs. Therefore, it is required to discover and develop MFCs anode materials with high conductivity, excellent electrochemical reversibility, stability, biocompatibility, exceptional microbial adhesion performance, commercial availability, and low cost (Duarte et al., 2019; Kalathil and Pant, 2016; Christwardana et al., 2023; Pisciotta et al., 2012; Rahimnejad et al., 2015).

Eggs are employed extensively in the culinary, medicinal, and industrial sectors, as well as in the home (Hadiyanto et al., 2021). However, after the eggs have been consumed, the eggshells are discarded as solid trash. A calcium carbonate matrix and a protein-rich fibrous membrane compose the eggshell. This biowaste is often disposed of in landfills, which incurs costs (Minakshi et al., 2018). Significant quantities of eggshell waste pose environmental and economic difficulties, as well as processing hurdles (Balasubramanian et al., 2020). Eggshells contain the greatest content of calcium carbonate (94 %) and calcium phosphate (1 %) according to Li et al. (2012). Compounds of tilleyite ($Ca_5Si_2O_7(CO_3)_2$) are also present in eggshell powder (Aigbodion et al., 2018). Eggshell waste has been used for a number of purposes, including bio-ceramics, bio-templates, cosmetics, and dye adsorbent (Murakami et al., 2007; Minakshi et al., 2018). Reusing waste may contribute to sustainable development by delivering economic and ecological benefits (Minakshi et al., 2019). According to the earlier article, eggshells may be converted into MFC anodes by calcination. In addition, 3D carbonized eggshells may be used as electrodes for high-performance supercapacitors (Li et al., 2012).

The calcined eggshell powder was successfully produced from eggshell utilizing a simple chemical activation method including sodium hydroxide as the activator (Ahmad et al., 2020). The structure of eggshell that had been crushed and calcined at 600 °C was calcite ($CaCO_3$) (Minakshi et al., 2019). $CaCO_3$ is a polymorph that occurs in three naturally occurring anhydrous crystalline forms: calcite, aragonite, and vaterite. Calcite is the most thermodynamically stable form of $CaCO_3$ at ambient temperature and atmospheric pressure (Gopinath et al., 2002). The exploitation of eggshell waste to make calcined eggshell powder has received little attention, and the lack of publications on this material has prompted interest in synthesizing eggshell powder from eggshell waste for MFC electrode applications (Balasubramanian et al., 2020).

The objective of this study is to synthesize calcination from eggshell waste utilizing different ratios of eggshell mass to NaOH as an activator to discover the most effective concentration variations for synthesizing calcined eggshell powder. The calcined eggshell powder generated will next be assessed for its physicochemical qualities and employed as anode material in yeast MFCs.The goal of this research is to determine the optimal yeast MFC power output utilizing calcined eggshell anodes with varying eggshell:NaOH ratios. The investigation of the variation of eggshell:NaOH ratio in the calcination process of eggshell as MFC anode has never been done previously, making this research an academic novelty. Utilizing calcined eggshell powder from eggshell waste is projected to be a cost-effective and green energy source option.

2. Materials and method

2.1. Eggshell calcination process

The eggshell calcination method adheres to the methodology used by Ahmad et al. (2020). Before being sun-dried for 24 h, the egg shells were washed in deionized (DI) water. The dried egg shells are then ground into fine powder using a blender or mortar. 100 mL of DI water was added after weighing the egg shells and NaOH in weight ratios of 1:4, 1:1, and 4:1. The mixture is then stirred for 1 h with a magnetic stirrer until it is homogeneous, after which it is kept at room temperature for 24 h to allow the activation process to finish. The mixture was thereafter filtered and washed thoroughly with DI water. The filtered solids were then calcined for 3 h at 550 °C in a furnace. Fig. S1 displays the whole process of calcining eggshells from beginning to finish.

2.2. Physicochemical analysis

X-ray diffractions Rigaku SmartLab SE (Tokyo, Japan) operating at 40 kV, 30 mA, and 5–80° (2 θ) with CuK as the radiation (λ = 1.5406 nm) was used to determine the crystalline morphology of the modified CF anodes. For FTIR measurements, a Compact FT-IR Spectrometer ALPHA II (Massachusetts, United States) was used. The morphology of the modified CF anode with calcined eggshell surface was examined using a FE-SEM FEI Quanta 650 (Oregon, United States). To increase the sample's conductivity, a double-sided conductive adhesive tape was applied. The SEM pictures were compared before and after the alteration process. Using a Malvern Mastersizer 3000 (Worcestershire, United Kingdom) with sieve sizes ranging from 20 to 200 mesh, the size distribution of raw and calcined eggshell particles was measured. A Nikon D5200 (Tokyo, Japan) DSLR camera was used to acquire photos perpendicular to the surface of the sample, and angles were determined by hand using a protractor. In this experiment, the surface area was determined using the equation devised by Maltsev et al. (2018) based on the reduction in methylene blue absorbance produced by changed materials' absorption. Synthesized sample UV–Vis absorption spectra were acquired between 300 and 800 nm using a twin beam UV–Vis spectrophotometer (Analytic Jena Specord 250).

2.3. Anode modification for single cell test

To evaluate the effectiveness of yeast MFC, modified Carbon Felt (CF) covered with calcined eggshell was used as the anode. CF with a projected surface area of 7 cm^2 was soaked in 1 M NaOH for 1 h and then rinsed with DI water for the first time (Zhou et al., 2006). The objective is to change CF from a hydrophobic to a hydrophilic condition such that it easily interacts with a solution containing calcined eggshell. To create a Nafion solution suitable for use as a binder, 5 % Nafion solution was dissolved in a 1:1 mixture of DI water and ethanol, which was then homogenized to a concentration of 0.05 %. The solution was then added to 1 $mg.mL^{-1}$ of calcined eggshell and ultrasonicated for 10 h until homogeneous, resulting in the formation of Nafion/calcined eggshell. After soaking the hydrophilic CF for 1 h in the mixture, the modified CF was washed to remove unbound calcined eggshell and dried overnight at 60 °C.

2.4. MFC Performance Test

This research employed use of a 28 mL-capacity acrylic MFC reactor.

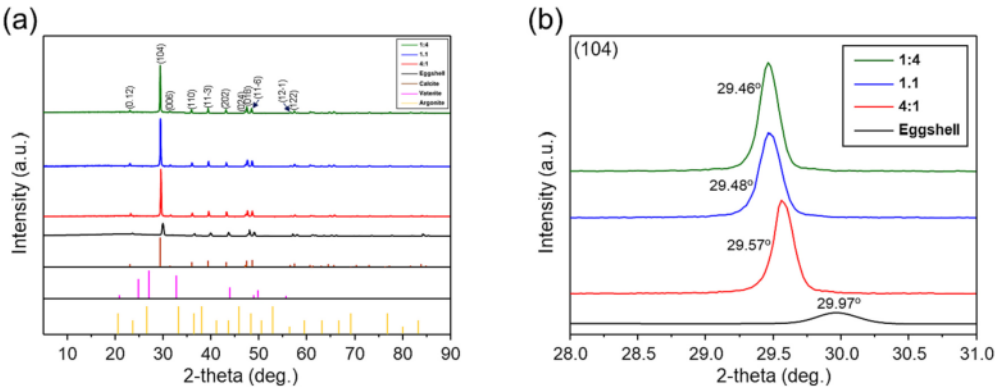

Fig. 1. XRD spectra of vaterite, calcite, raw and calcined eggshell.

The anode is made up of modified CF with calcined eggshell, whereas the cathode is made up of plain CF. The projected surface area of the two electrodes is 7 cm^2 with a distance between them of about 10 cm. The anode and cathode compartments were separated using a Nafion 117 membrane. The anode compartment was filled with a total of 28 mL of anolyte in the form of a biocatalyst and Yeast extract – Peptone – D-glucose (YPD) medium containing 14 $mg.mL^{-1}$ yeast *Saccharomyces cerevisiae*, 14 $mg.mL^{-1}$ D-glucose, 5 $mg.mL^{-1}$ yeast extract, and 2.5 $mg.mL^{-1}$ peptone (Christwardana et al., 2018). In the meanwhile, the oxygen reduction reaction proceeds when the cathode is in direct contact with air (ORR). During the incubation phase, stainless steel wire is used as the current collector, and the anode and cathode are linked to a 1000 Ω external resistance. Throughout the 30 days of incubation, voltage measurements were obtained three days every cycle (total 10 cycles). In the first three cycles, yeast and YPD medium replaced anolyte. Following this, the anolyte was replaced with D-glucose, assuming that a mature biofilm had developed over the course of the previous three cycles. The Maximum Power Density (MPD) is calculated from the polarization and power curves by multiplying the voltage by the current density for different external resistance variations. A resistor box (Elenco RS500 Resistance Substitution Box, Illinois, USA) was connected between the yeast MFC's anode and cathode after 10th cycle, and setting it to 10 MΩ-10 Ω for 30 min every value. During which time the data collection system recorded the output voltage every 10 min.

2.5. Density functional theory (DFT) calculations

All DFT calculations were calculated using the spin-polarized generalized gradient approximation (GGA) of the Perdew–Burke–Ernzerhof (PBE) function, which was performed in the DMol3 Package. The calcite crystal structure was built from an trigonal rhombohedral structure and a space group of *R-3c* (a = 4.207 Å, b = 4.207 Å, c = 17.151 Å for raw eggshell and a = 4.311 Å, b = 4.311 Å, c = 17.029 Å for 4:1 sample) for geometry optimization. The Calcite structures were relaxed for the calculations using a 4 × 4 × 2 k-point set and the self-consistent field (SCF) tolerance was set to 1×10^{-6} eV per atom with a maximum force of 0.05 eV $Å^{-1}$ and maximum displacement of 0.005 Å.

3. Results and discussion

3.1. XRD analysis

3.1.1. Crystal structure analysis

Fig. 1a shows the XRD patterns of raw eggshell and calcined eggshell powder with NaOH activator at varying mass ratios (1:4, 1:1, and 4:1) as well as the simulated spectra of calcite, vaterite, and aragonite. $CaCO_3$ possesses polymorphic crystal formations, meaning it may exist in several crystal forms (Gopinath et al., 2002; Minakshi et al., 2019). $CaCO_3$ exists in three crystal forms: calcite, vaterite, and aragonite. However, calcite forms are the most prevalent because their structure is the most stable (Xu et al., 2005). In addition, the XRD data of whole samples were compared with ICDD (International Center for Diffraction Data) cards of Calcite (ICDD card No. 00-047-1743), vaterite (ICDD card No. 01-072-0506), and aragonite (ICDD card No. 01-072-0506) to guarantee the crystal form of samples (Khan et al., 2019; Khan et al., 2020). Fig. 1a depicts the XRD peak locations of complete samples that match to the calcite polymorph and are indexed as trigonal-rhombohedral with a space group of R-3c (Sudheesh Kumar et al., 2013). In comparison to eggshell samples activated with NaOH, the raw eggshell sample exhibits larger peaks, demonstrating its poor crystallinity. As indicated in Table 1, the lattice parameter of whole samples follows the same pattern as the ICCD of calcite polymorph. The lattice parameter a = b tends to increase with increasing NaOH activator concentration, resulting in cell volume expansion. The increase in lattice characteristics and cell volume may diminish the favorable electron migration in anode applications (Choi et al., 2022).

Table 1
Crystal lattice parameter of calcined eggshell powder.

Material	a (Å)	b (Å)	c (Å)	V (Å)
ICDD 00-047-1743 (Calcite)	4.990	4.990	17.061	424.82
ICDD 01-072-0506 (Vaterite)	4.13	4.13	8.49	144.81
ICDD 00-003-0425 (Argonite)	4.955	7.9610	5.7360	226.27
Raw eggshell powder	4.207	4.207	17.151	303.55
Sample 4:1	4.309	4.309	17.019	316
Sample 1:1	4.310	4.310	17.022	316.20
Sample 1:4	4.311	4.311	17.029	316.48

*ICCD = International Center for Diffraction Data.

Fig. 1b shows a magnification image of the (104) peak from entire sample. As the NaOH ratio rises, the (104) peak changes to a lower angle, suggesting an increase in the lattice size of the (104) plane. The lattice size of (104) plane of entire samples can be determined by the Bragg Eq. (1):

$$d_{104} = \frac{\lambda}{2\sin\theta} \quad (1)$$

where d_{104} is the lattice size of the (104) plane, λ is the wavelength of the XRD light source (Cu = 1.5406 nm), and θ is the diffraction angle of the (104) plane (He et al., 2018). Table S1 displays the computed lattice size of the entire sample set. The presence of the NaOH activator led to the absorption of sodium ions into the pores of the eggshell powder, which resulted in the opening of the lattice fringes of the sample during the

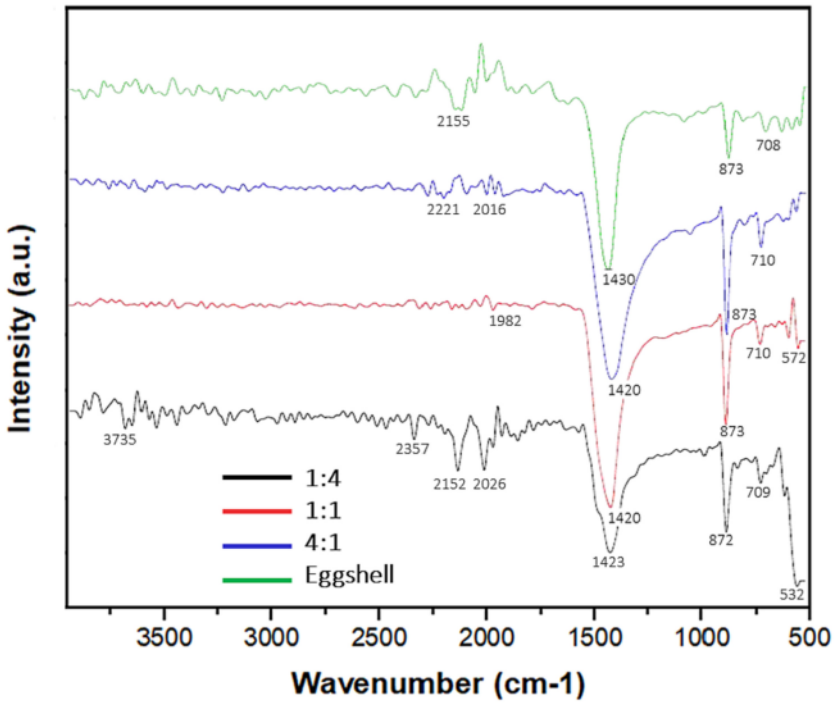

Fig. 2. FTIR spectra from raw and calcined eggshell.

calcination process. This process is hastened by the creation of H2O gas, which dissolves the remaining hydrocarbon molecules on the eggshell powder's surface (Awogbemi et al., 2020). In addition, this activation may remove impurities such as silica and ash from the surface of eggshell powder, resulting in an increase in surface area and porosity (Ahmad et al., 2020; Owuamanam and Cree, 2020).Glukhovsky (1967) and Krivenko (1994) suggested a model for alkaline activation of silica and lime-rich materials based on a sequence of processes outlined below (Eqs. (2)–(4)):

$$= Si - O^- - + R^+ == Si - O - R \quad (2)$$

$$= Si - O - R + OH^- == Si - O - R - OH^- \quad (3)$$

$$= Si - O - OH - + Ca^{2+} == Si - O - Ca - OH + R^+ \quad (4)$$

During the first phase of hydration, the basic cation (R^+) acts as a catalyst by cationic exchange with Ca^{2+} ions. During the course of the chemical reaction, the structure is filled with basic cations. Palomo et al. (2004) and Fernández-Jiménez et al. (2003) found that the composition of the alkaline solution greatly impacted the activation, particularly at the onset and in the setting of the paste. The activation of alkaline slag is a multistage process beginning with the slag's breakdown and concluding with the polycondensation of reaction products (Li et al., 2010). In combination with a variety of secondary products, the major reaction product, a gel whose composition and structure vary depending on the usual calcium silicate hydrate (CSH) generated during OPC hydration, is formed. Numerous variables impact the sort of secondary product produced, including the starting material's composition, the type and concentration of the activator, the storage conditions, and the pH (Garcia-Lodeiro et al., 2015).

3.1.2. Crystal grain size analysis

The crystal grain size distribution of samples can be calculated by Debye–Sherer equation (Eq. (5)):

$$D = \frac{k\lambda}{\beta \cos\theta} \quad (5)$$

where k is the shape factor (0.9), λ is the wavelength of the XRD light source (Cu = 1.5406 nm), β is the width of the peak at full width at half maximum (FWHM), and θ is the diffraction angle of the peak. Table S2 displays the computed crystal grain size for all of the samples. The crystal grain size of the sample of raw eggshell powder was measured to be 23.91 nm. In general, increasing the NaOH concentration throughout the synthesis process causes the crystal grains to grow in size. In the 4:1, 1:1, and 1:4 samples, the crystal grain size increased by about 71.47, 85.59, and 145.19 nm, respectively. Increasing the NaOH activator causes the crystal grains to expand, suggesting enhanced crystal formation. The increased stiffness of the sample corresponded to the larger size of the crystals (Liu et al., 2013). It is well-established that modifying the crystal size has no noticeable effect on the anode's most important characteristic, namely electron conductivity (Lee et al., 2014).

3.1.3. Crystallinity analysis

Comparing the peak area of the crystal phase to the total area of the graph from the XRD spectra reveals the degree of the test sample's tendency to crystallize. In Table S3, the crystallinity of the test samples is summarized. After the activation and calcination operations, the crystallinity was determined to have risen. The crystallization percentage of raw eggshell powder is 29.49 %, but the crystallization percentage of the 4:1 sample is 38.93 %. The crystallinity of the 1:1 sample is virtually identical to that of the 4:1 sample, which is 39.65 %. Due to the addition of the NaOH concentration, however, the 1:4 sample exhibits a crystallinity of 43.92 %. Crystallinity is a sign of a particle having a constant spatial arrangement (Zhao et al., 2020). The crystallinity value also affects the sample's conductivity, which grows as crystallinity increases (Diantoro et al., 2017).

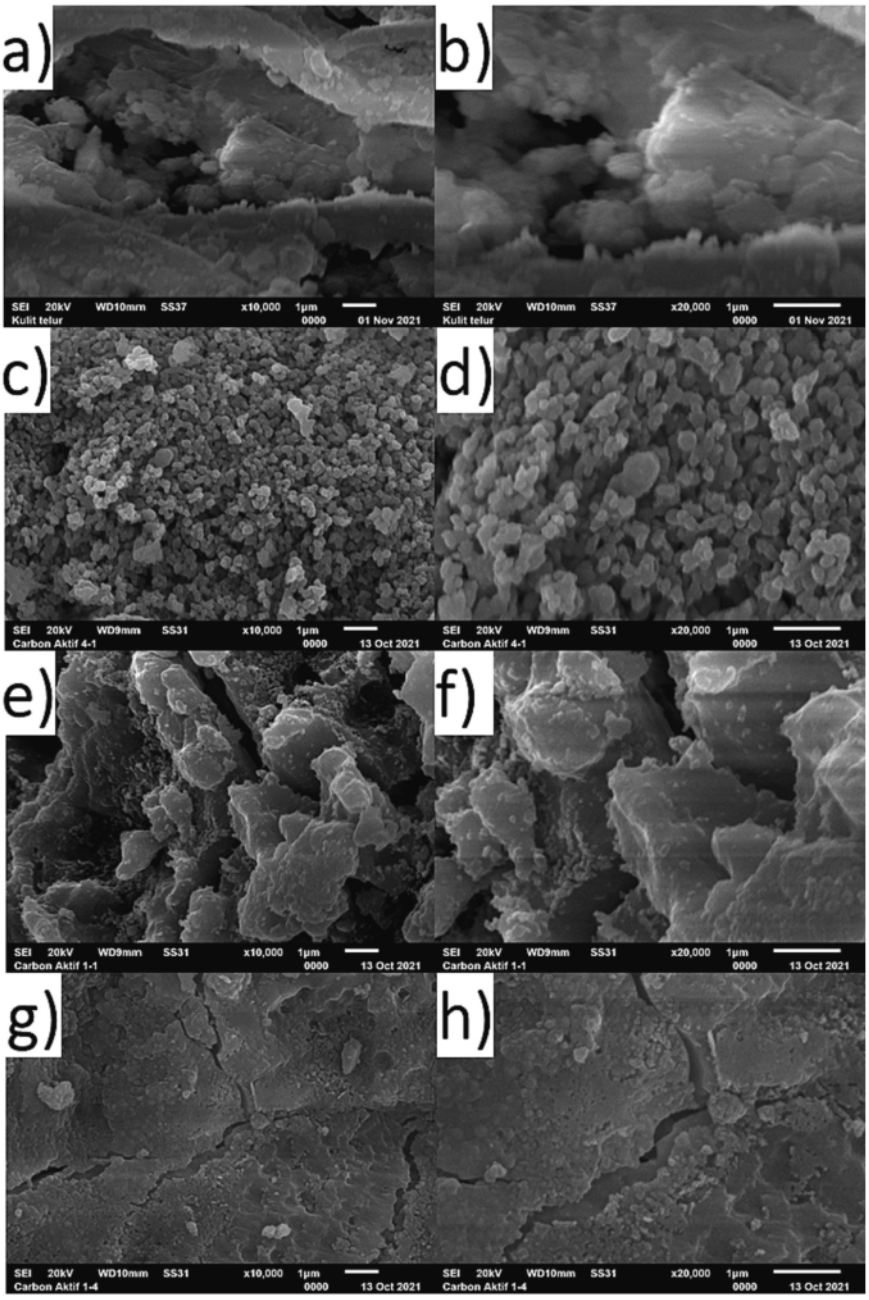

Fig. 3. The morphology of a) raw eggshell and calcined eggshell with eggshell-NaOH ratio of c) 4:1, e) 1:1, and g) 1:4 at 1000× magnification. While b), d), f), and h) are their morphology respectively at 2000× magnification.

3.2. FTIR analysis

Utilizing FTIR spectroscopy, the functional groups and chemical components of calcined egg powder were analyzed. Fig. 2 shows the FTIR spectra of each sample. Only eggshell samples had the chemical group hydroxyl, as indicated by wave number 3265 cm^{-1} (Ahmad et al., 2020). At wave number 3265 cm^{-1}, no peak was seen in samples 1:4, 1:1, or 4:1, suggesting that the hydroxyl group has been eliminated by NaOH activation and calcination. In addition, the figure illustrates that all samples maintain carbonate ions, calcium oxide, and calcium carbonate after NaOH activation and calcination. The greatest peak appears between 1421 and 1439 cm^{-1}, suggesting the presence of carbonate ions in all samples (Nandiyanto et al., 2019). Carbonate ions are also identified at wave number 873–879 cm^{-1} in all test samples (Nandiyanto et al., 2019). All test samples with the wave number 528–611 cm^{-1} include calcium oxide as a secondary component (Amarasinghe and

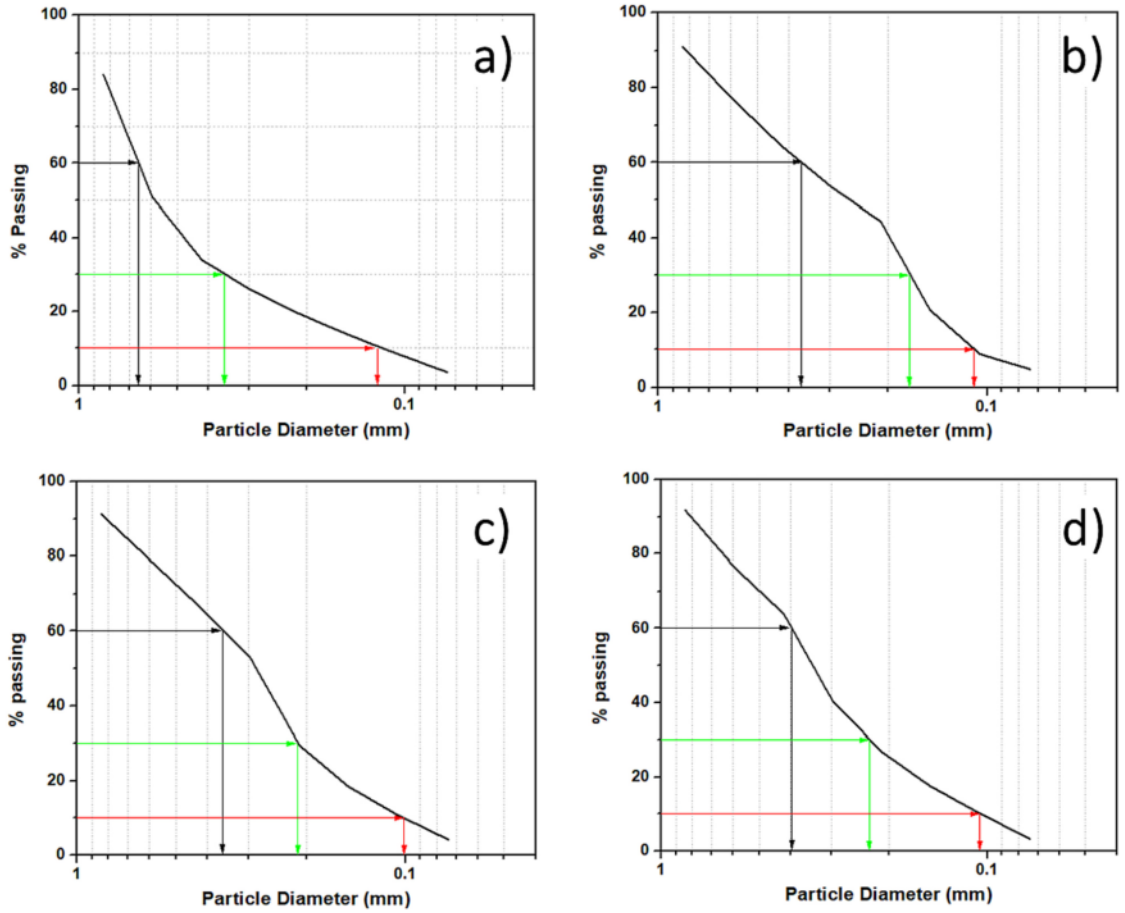

Fig. 4. Particle Size Distribution curves of a) raw eggshell and calcined eggshell with eggshell-NaOH ratio of b) 4:1, c) 1:1, and d) 1:4.

Wanniarachchi, 2019). At wave number 709–709 cm^{-1}, calcium carbonate was identified as the major constituent of both the eggshell and calcined test sample (Tsai et al., 2006).

3.3. SEM analysis

The form represented in Fig. 3 was revealed by scanning electron microscopy (SEM) examination of the calcined eggshell powder sample activated with NaOH. Fig. 3a and b depict eggshell powder samples with sizes of 1000× and 2000×, respectively. As can be seen, the eggshell powder's surface is not hollow. The samples shown in Fig. 3c and d are calcined egg shells with a 4:1 ratio and 1000× and 2000× magnifications; the surface is highly uneven and the roughness is pretty substantial. Fig. 4e and f show calcined eggshell samples with a 1:1 ratio of 1000× and 2000×, respectively; the surface is smoother than with a 4:1 ratio. Fig. 4g and h depict a calcined eggshell sample with a 1:4 ratio and 1000× and 2000× magnifications; the surface is not rough, aggregation forms owing to the high concentration of NaOH, and a portion of the surface seems broken.

Table 2
Particle size distribution results from raw and calcined eggshell powder.

Parameters	Eggshell	4:1	1:1	1:4
% Gravel	15.87	8.93	8.83	8.32
% Sand	80.70	86.32	86.98	88.47
% Fines	3.43	4.75	4.19	3.21
D60 (mm)	0.66	0.37	0.37	0.40
D30 (mm)	0.36	0.17	0.22	0.23
D10 (mm)	0.12	0.11	0.11	0.10
Cu	5.56	3.36	3.38	3.81
Cc	1.64	0.74	1.19	1.28

*Cu = uniformity coefficient; Cc = curvature coefficient.

The eggshell's form indicates the presence of a porous structure. This means that the sample includes egg membrane fragments (Daraei et al., 2014). The eggshell sample possesses a high degree of crystallinity, as shown by its monolithic form (Kavitha et al., 2019). From a morphological standpoint, the calcined eggshell has an irregular shape. The discovery of eggshells that had been calcined revealed an irregular calcite structure. The process of calcination increases the surface area (Ahmad et al., 2020). In calcination, the synthesis temperature is a critical factor. This surface is where the active site is produced by surface-level activities. The active site is a process for material absorption that leads to the creation of micropores in activated carbon (Pezoti et al., 2016). Calcined egg shells have a rather rough surface, which facilitates increased cell/bacteria adherence to the anode. Greater roughness and porosity on anodes increases their ability to bind pathogens (Lu et al., 2015). The number of electrons carried from the anode to the cathode rises as a consequence of the increased surface area of the calcined eggshell powder.

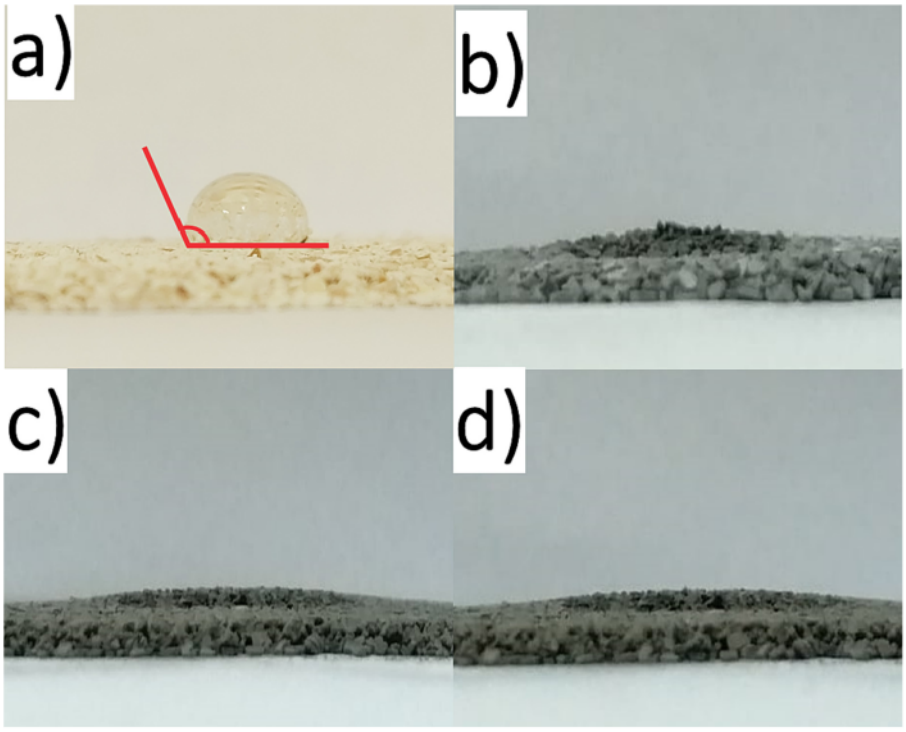

Fig. 5. Contact angle of a) raw eggshell and calcined eggshell with eggshell-NaOH ratio of b) 4:1, c) 1:1, and d) 1:4.

3.4. Particle size distribution

As an activator, the addition of NaOH affected the particle size distribution. The particle distribution for each sample is visually shown in Fig. 4. Fig. 4a shows a graph of chicken eggshell samples, while Fig. 4b, c, and d illustrate, respectively, a 4:1, 1:1, and 1:4 ratio. The black arrows reflect the sample distribution at d60, the green arrows represent the sample distribution at d30, and the red arrows represent the sample distribution at d10. The graph demonstrates that the proportion of particles passing through a filter increases with decreasing particle size (Chaudemanche et al., 2018). To generate nanoparticles, particle size reduction may be achieved by milling for several hours (Hernández-Varela et al., 2021). Table 2 provides a summary of the findings of the particle dispersion analysis conducted on each analyzed sample. Eggshells have the biggest percentage of size, followed by 4:1, 1:1, and 1:4, with the particle dispersion becoming finer as the NaOH concentration is increased. Due to the alkaline nature of each sample, finer particles may be lost during washing. Ławińska et al. (2020) note that particle size might be lost during the weighing analysis procedure. The distribution of 60 mm and 10 mm samples demonstrates an unstable particle distribution that oscillates significantly up and down with a trend that is ambiguous. At a particle size of 30 mm, the distribution of particles becomes stable, and the larger the concentration of NaOH, the more uniform the particle distribution. The uniformity coefficient (Cu) of calcined eggshell is less than 4, but it is more than 4 for raw eggshell. This illustrates that the calcination process has an effect on the particle distribution uniformity, as confirmed by the curvature coefficient (Cc) data.

3.5. Surface area and contact angle analysis

Indirectly determining the surface area by measuring the absorbance of methylene blue absorbed by the sample using the UV–Vis spectrometer (Maltsev et al., 2018). On the basis of these observational data, the concentration of the absorbed solution in the sample was calculated. The surface area was calculated using the extension coefficients of the 612 nm and 664 nm wavelengths, which are respectively 9.95 and 6.60. A chicken eggshell powder sample had a surface area of 179.1 $m^2.g^{-1}$, whereas a sample with a ratio of 1:4 produced 181.2 $m^2.g^{-1}$, a sample with a ratio of 1:1 produced 180.6 $m^2.g^{-1}$, and a sample with a ratio of 4:1 produced 180.7 $m^2.g^{-1}$. Compared to the other three samples, the sample of laminated egg shells with a ratio of 1:4 produced the greatest surface area, which was 181.2 $m^2.g^{-1}$. These findings are comparable to those of several prior studies (Tseng et al., 2014; Ma and Hou, 2019; Sami et al., 2018). When used as an anode in an MFC circuit, the sample's surface area influences its absorption. Because a bigger surface area contains more surfaces that may absorb electrons or microbes, more electrons are transferred from the anode to the cathode, resulting in an increase in the MFC's power output (Logan, 2008).

Fig. 5 depicts the examination of each sample's contact angle. As seen in the eggshell powder sample, water that is put on the surface does not absorb but instead generates water droplets with a contact angle of 115° from the surface (Fig. 5a). Due to the eggshell powder sample's hydrophobic characteristics, it is not suited for use as an anode in an MFC since electrons and microbes would have difficulty absorbing in the electrode. When water was dropped on the 4:1, 1:1, and 1:4 samples, no droplets formed (Fig. 5b, c, and d). This shows that all calcined eggshell samples are hydrophilic, since the samples' rapid absorption improves the absorption of electrons and microbes, leading in enhanced electron transfer from anode to cathode and enhanced MFC power output (Kim et al., 2011). Changes in the anode's physical features, from hydrophobic to hydrophilic, prompted the formation of yeast colonies during the biofilm formation process (Christwardana et al., 2022).

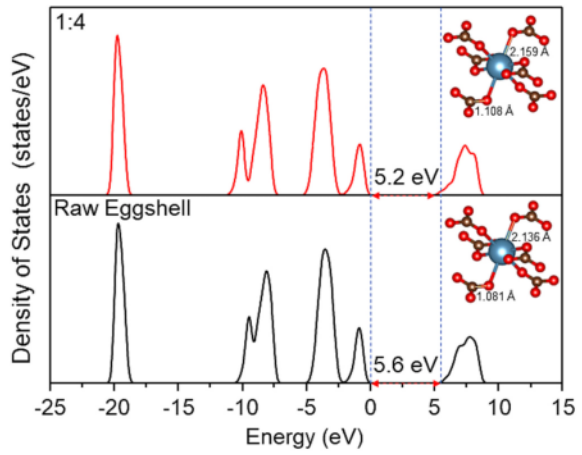

Fig. 6. Density state of raw eggshell and calcined eggshell with eggshell-NaOH ratio of 1:4.

3.6. DFT calculation

Calculations based on the density functional theory (DFT) are used to explain the impact of increased lattice parameters of samples caused by a rise in NaOH concentration. Fig. 7 depicts the total density of states (TDOS) of raw eggshells and 1:4 samples. From raw eggshell, the band gap of sample 1 to sample 4 fell to 5.2 eV. (5.6 eV). This diminishing band gap suggests that the 1:4 sample gets more conductive, which may improve the sample's performance as an anode in MFCs (Yaqoob et al., 2021). Fig. 6's inset depicts the increased a-b lattice parameters responsible for the increased interatomic distance between C—O and Ca—O bonds in raw eggshells. The binding force between valence electrons and atoms decreases as a consequence. When the valence electrons become less bonded by increasing the interatomic distance, the energy needed to set them free in the conduction band decreases, or the band gap energy decreases (Mir and Gupta, 2019). These explanations are correlated with the equation of crystal momentum of $k = 2\pi/a$ at the Brillouin-zone edge. Where k is the wave vector, π is pi constant (approximately 3.14), and a is lattice parameter "a" (Das et al., 2019). The bandgap energy can be calculated from the different energy between the lowest of the conduction band and highest valence band. These change in energy is attributed to a change in k from the de Broglie relations (Eq. 6):

$$\Delta E = \frac{p^2}{2m} = \frac{(\hbar k)^2}{2m} \tag{6}$$

Based on these equations, when the lattice parameter "a" increased, the wave vector of k will be decreased which also make the energy gap decrease (Williams et al., 2012).

3.7. UV–Vis and band-gap analysis

Fig. 7a illustrates the UV–Vis spectroscopy results. The movement of electrons from the valence band to the conduction band is responsible for the approximately 450 and 350 nm absorption band thresholds of calcined and raw eggshell, respectively. This demonstrates that activation and calcination changed the fundamental band structure of eggshell. With increasing NaOH as an activator and calcination technique, however, a unique transformation occurred, as is normal when semiconductors undergo transformations. This peak represents strain-induced modifications to the electronic structure of activated and calcined eggshell.

The alteration of the absorption edge resulting from the activation and calcination processes is reflected immediately in the band gap energy. Taking into account the importance of indirect allowed transition (Khan et al., 2015; Xiong et al., 2010) we set m = 0.5 and plotted the curves of $(\alpha h\upsilon)^{0.5}$ against hυ, where is the absorption coefficient and hυ is the photon energy. The values of E_g were then determined by separating the linear section of the curves to $(\alpha h\upsilon)^{0.5} = 0$. Regarding the eggshell minerals calcite, veterite, and argonite, both activated and calcined eggshells revealed decreased E_g values in the range of 2.33 eV

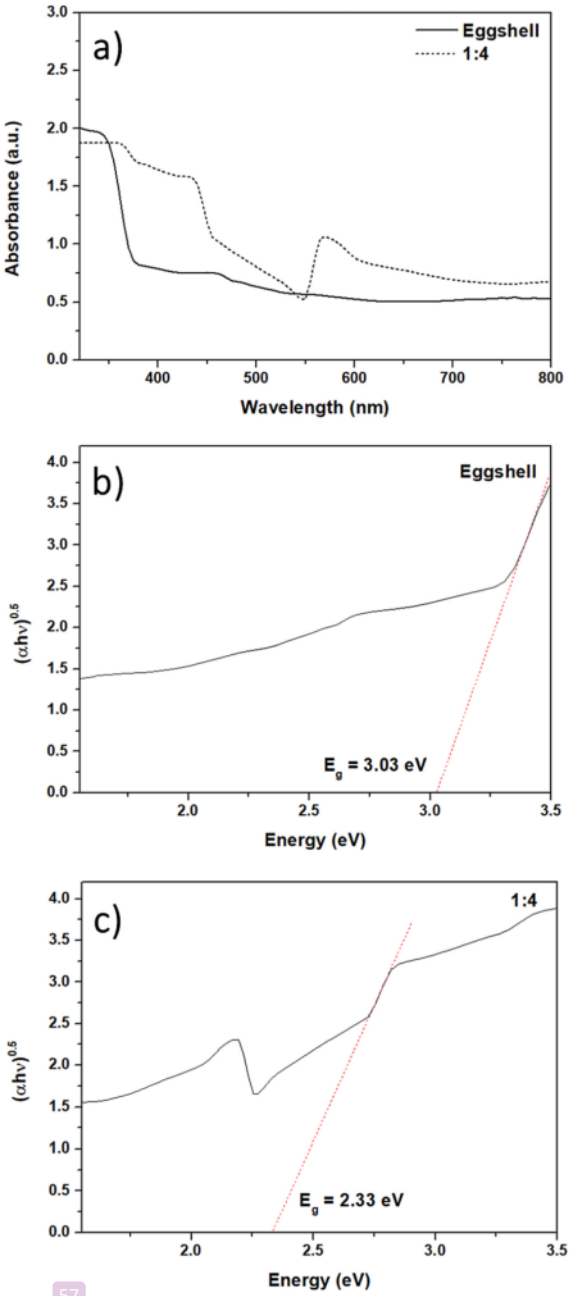

Fig. 7. a) UV–Vis spectra and Tauc plot of b) raw eggshell and c) calcined eggshell with eggshell-NaOH ratio of 1:4.

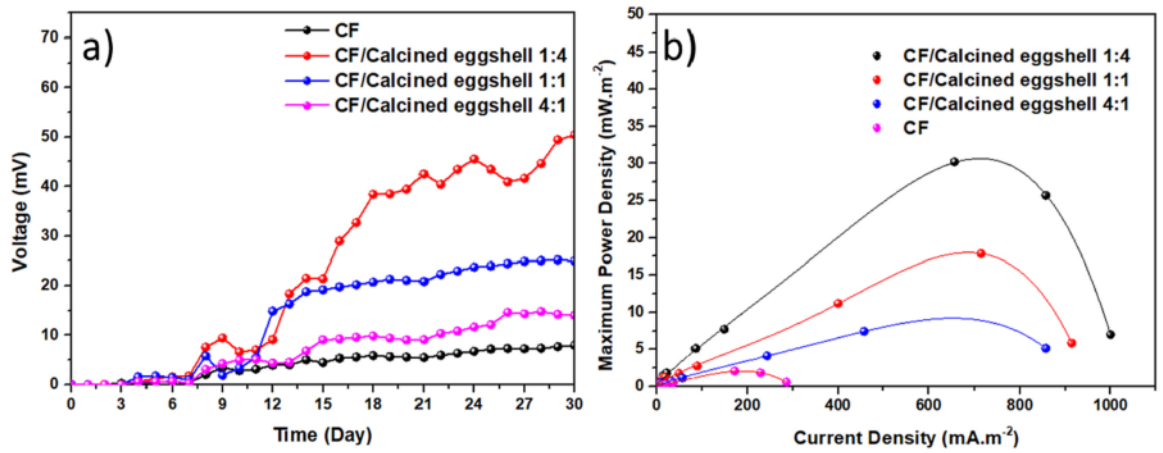

Fig. 8. a) voltage and b) power curves of yeast MFC employing calcined eggshell @ CF as anode.

Table 3
Comparison of MFC performance to several earlier studies.

Anode	Cathode	Substrate	Total operation time (day)	MPD (mW. m^{-2})	Reference
Graphite felt	SS mesh	Urine waste	15	46.97	Apollon et al. (2023)
Graphite rod	Graphite rod	Potato waste	20	36.84	Yaqoob et al. (2022)
Graphite granule	Carbon felt	Synthetic wastewater	98	−8.84 (33.14 mW. m^{-3})	Gupta et al. (2021)
Graphite felt	Zinch sheet	Garden soil with NH_4NO_3	270	2.76	Apollon et al. (2022a, 2022b)
Calcined eggshell@carbon felt	Carbon felt	YPD medium (Glucose)	30	31	This work

(Fig. 7c), which is about 23 % lower than raw eggshell, which has an energy band gap of around 3.0 eV. (Fig. 7b). In addition to phase composition, film density (Mechiakh et al., 2010; Mathews and Morales, 2009), grain size (Nair et al., 2011), and surface topography (Xi et al., 2017) have been shown to impact Eg. Despite a difference in the final value, the trend of this Eg result is consistent with the trend of Eg in the prior section's DFT calculation.

3.8. Full cell analysis

Ten consecutive batch cycles were performed on the MFC, and the steady-state voltage trend is shown in Fig. 8a. The beginning duration for MFCs with calcined eggshell anodes was much shorter (6 h) than that of the control CF anode (i.e., 12 h). The CF anode coated with calcined eggshell 1:4 displayed the greatest maximum voltage (i.e., ~45 mV), which was 5.6-fold higher than the control anode (~8 mV), showing that calcined eggshell had a greater affinity as an anode for fungal attachment. Although CF has been frequently used as an anode in MFCs due to its simplicity and cheap cost, its decreased surface area when compared to CF with modified calcined eggshells results in restricted bacterial adhesion and the formation of a scattered biofilm structure (Guo et al., 2013). Our results suggest that calcined eggshell doping may significantly increase the conductivity and biocompatibility of carbon-felt electrodes by increasing the surface area and adhesion ability with yeast to form biofilms, hence generating larger current densities. MFCs with CF anodes embedded with calcined eggshell 1:4 exhibited the maximum power density (i.e., 31 $mW.m^{-2}$), which was 14.8-times more than MFCs with CF anodes having an MPD value of 2.1 $mW.m^{-2}$ (Fig. 8b). The power densities of MFCs with calcined eggshell 1:1 and 4:1 modified CF anodes are 18 and 9.2 $mW.m^{-2}$, respectively. In addition, the internal resistance of each MFC was determined by extrapolating the linear zone of the overall MFC polarization curve (Mahmoud et al., 2011), since it is evident that the internal resistance frequently limits the generation of high power and current density in the MFC (Pérez-Rodríguez et al., 2016). MFCs with calcined eggshell 1:4 anodes had the lowest internal resistance of 160 Ω compared to control MFCs (196 Ω), calcined eggshell 1:1 (239 Ω), and calcined eggshell 4:1 (250 Ω). This is likely the reason for calcined eggshell 1:4's higher efficiency compared to others. The power output findings of this investigation are comparable to those of several previous studies, as indicated in Table 3. As demonstrated in Table 3, the MPD value is affected by a number of variables, including electrode material, substrate, biocatalyst, operating conditions, construction, and the MFC system.

4. Conclusion

The effect of eggshell-to-NaOH ratio on the structure, morphology, and electrochemical performance of calcined eggshell anode materials for yeast MFC was investigated methodically. The results reveal that the ratio of eggshell to NaOH influences the chemical, physical, and electrochemical characteristics of calcined eggshell. When the activator concentration of NaOH is enhanced, crystal size and crystallinity both increase. This may increase electron transport, hence enhancing conductivity. Density Functional Theory suggests that calcined eggshell with a 1:4 ratio may reduce band gap energy in comparison to uncalcined eggshell. A ratio of 1:4 of calcined eggshell to yeast MFC yields in excellent performance, as seen by the relatively high voltage and maximum power density produced in comparison to the control CF. This indicates that calcined eggshell accelerates electron transport in the yeast MFC system. While synthesizing calcined eggshell anode materials, it is crucial to optimize the synthetic conditions, such as the concentration of NaOH as an activator. The ideal eggshell-to-NaOH ratio affects the anode's structure and composition, which must be investigated carefully during the synthesis of different calcined eggshell anode materials to maximize their electrochemical performance.

CRediT authorship contribution statement

Conceptualization, M.C.; data curation, M.C., J.J., S.K.; formal analysis, M.C., J.J., S.K., and A.Y.M.; funding acquisition, M.C.; investigation, M.C., A.Y.M.; methodology, M.C.; validation, A.Y.M.; visualization, M.C., A.Y.M.; writing - original draft, M.C., A.Y.M.; writing – review and editing, M.C. All authors have read and agreed to be published version of the manuscript.

Declaration of competing interest

The authors declare that they have no known competing financial interests or personal relationships that could have appeared to influence the work reported in this paper.

Data availability

Data will be made available on request.

Acknowledgement

This research fully funded by Badan Riset dan Inovasi Nasional (BRIN) and Lembaga Pengelola Dana Pendidikan (LPDP) - The Ministry of Finance through scheme Riset dan Inovasi untuk Indonesia Maju (RIIM) Batch 2 (No. 93/IV/KS/11/2022 and 652/UN7.D2/KS/XI/2022).

Appendix A. Supplementary data

Supplementary data to this article can be found online at https://doi.org/10.1016/j.biteb.2023.101347.

References

Ahmad, A., Jini, D., Aravind, M., Parvathiraja, C., Ali, R., Kiyani, M.Z., Alothman, A., 2020. A novel study on synthesis of egg shell based activated carbon for degradation of methylene blue via photocatalysis. Arab. J. Chem. 13 (12), 8717–8722.

Aigbodion, V.S., Edokpia, R.O., Asuke, F., Eke, M.N., 2018. Development of egg shell powder solution as ecofriendly reagent: for chemical treatment of natural fibers for polymer composites production. J.Mater.Environ.Sci. 9 (2), 559–564.

Amarasinghe, A., Wanniarachchi, D., 2019. Eco-Friendly photocatalyst derived from egg shell waste for dye degradation. J. Chem. 2019, 8184732.

Apollon, W., Rusyn, I., González-Gamboa, N., Kuleshova, T., Luna-Maldonado, A.I., Vidales-Contreras, J.A., Kamaraj, S.K., 2022. Improvement of zero waste sustainable recovery using microbial energy generation systems: a comprehensive review. Sci. Total Environ. 817, 153055.

Apollon, W., Valera-Montero, L.L., Perales-Segovia, C., Maldonado-Ruelas, V.A., Ortiz-Medina, R.A., Gómez-Leyva, J.F., Kamaraj, S.K., 2022. Sustain.Energy Technol. Assess. 49, 101730.

Apollon, W., Luna-Maldonado, A.I., Kamaraj, S.K., Vidales-Contreras, J.A., Rodríguez-Fuentes, H., Gómez-Leyva, J.F., Ortiz-Medina, R.A., 2023. Self-sustainable nutrient recovery associated to power generation from livestock's urine using plant-based bio-batteries. Fuel 332, 126252.

Awogbemi, O., Inambao, F., Onuh, E.I., 2020. Modification and characterization of chicken eggshell for possible catalytic applications. Heliyon 6 (10), e05283.

Balasubramanian, V., Daniel, T., Henry, J., Sivakumar, G., Mohanraj, K., 2020. Electrochemical performances of activated carbon prepared using eggshell waste. SN Appl.Sci. 2 (1), 1–12.

Chaudemanche, S., Perrot, A., Pimbert, S., Lecompte, T., Faure, F., 2018. Properties of an industrial extruded HDPE-WPC: the effect of the size distribution of wood flour particles. Constr. Build. Mater. 162, 543–552.

Choi, H., Kim, T., Park, H., 2022. Defect engineering of TiNb2O7 compound for enhanced Li-ion battery anode performances. Electrochim. Acta 404, 139603.

Christwardana, M., Frattini, D., Accardo, G., Yoon, S.P., Kwon, Y., 2018. Optimization of glucose concentration and glucose/yeast ratio in yeast microbial fuel cell using response surface methodology approach. J. Power Sources 402, 402–412.

Christwardana, M., Handayani, A.S., Yudianti, R., Joelianingsih, J., 2021. Cellulose-carrageenan coated carbon felt as potential anode structure for yeast microbial fuel cell. Int.J.Hydrog. Energy 46 (8), 6076–6086.

Christwardana, M., Joelianingsih, J., Yoshi, L.A., 2022. A novel of 2D–3D combination carbon electrode to improve yeast microbial fuel cell performance. J. Appl. Electrochem. 52 (5), 801–812.

Christwardana, M., Timuda, G.E., Darsono, N., Widodo, H., Kurniawan, K., Khaerudini, D.S., 2023. Fabrication of a polyvinyl alcohol-bentonite composite coated on a carbon felt anode for improving yeast microbial fuel cell performance. J. Power Sources 555, 232366.

Daraei, H., Mittal, A., Mittal, J., Kamali, H., 2014. Optimization of Cr (VI) removal onto biosorbent eggshell membrane: experimental & theoretical approaches. Desalin. Water Treat. 52 (7–9), 1307–1315.

Das, S., Gupta, G., Majumdar, K., 2019. Layer degree of freedom for excitons in transition metal dichalcogenides. Phys. Rev. B 99 (16), 165411.

Davis, J.B., Yarbrough Jr., H.F., 1962. Preliminary experiments on a microbial fuel cell. Science 137 (3530), 615–616.

Diantoro, M., Fitriana, I.N., Parasmayanti, F., Taufiq, A., Mufti, N., Nur, H., 2017. Crystallinity and electrical conductivity of PAN1-Ag/Ni film: the role of ultrasonic and silver doped. In: IOP Conference Series: Materials Science and Engineering, Vol. 202. IOP Publishing, p. 012005. No. 1.

Duarte, K.D., Frattini, D., Kwon, Y., 2019. High performance yeast-based microbial fuel cells by surfactant-mediated gold nanoparticles grown atop a carbon felt anode. Appl. Energy 256, 113912.

Fernández-Jiménez, A., Puertas, F., Sobrados, I., Sanz, J., 2003. Structure of calcium silicate hydrates formed in alkaline-activated slag: influence of the type of alkaline activator. J. Am. Ceram. Soc. 86 (8), 1389–1394.

Garcia-Lodeiro, I., Palomo, A., Fernández-Jiménez, A., 2015. An overview of the chemistry of alkali-activated cement-based binders. In: Handbook of Alkali-activated Cements, Mortars And Concretes, pp. 19–47.

Glukhovsky, V.D., 1967. Soil Silicate Articles And Structures. Budivel'nyk Publish., Kiev. Russian.

Gong, X., Peng, L., Wang, X., Wu, L., Liu, Y., 2020. Duckweed derived nitrogen self-doped porous carbon materials as cost-effective electrocatalysts for oxygen reduction reaction in microbial fuel cells. Int. J. Hydrog. Energy 45 (30), 15336–15345.

Gopinath, C.S., Hegde, S.G., Ramaswamy, A.V., Mahapatra, S., 2002. Photoemission studies of polymorphic CaCO3 materials. Mater. Res. Bull. 37 (7), 1323–1332.

Guo, K., Freguia, S., Dennis, P.G., Chen, X., Donose, B.C., Keller, J., Rabaey, K., 2013. Effects of surface charge and hydrophobicity on anodic biofilm formation, community composition, and current generation in bioelectrochemical systems. Environ.Sci.Technol. 47 (13), 7563–7570.

Gupta, S., Nayak, A., Roy, C., Yadav, A.K., 2021. An algal assisted constructed wetland-microbial fuel cell integrated with sand filter for efficient wastewater treatment and electricity production. Chemosphere 263, 128132.

Hadiyanto, H., Christwardana, M., Widayat, W., Jati, A.K., Laes, S.I., 2021. Optimization of flocculation efficiency and settling time using chitosan and eggshell as bio-flocculant in Chlorella pyrenoidosa harvesting process. Environ.Technol.Innov. 24, 101959.

He, K., Chen, N., Wang, C., Wei, L., Chen, J., 2018. Method for determining crystal grain size by X-ray diffraction. Cryst. Res. Technol. 53 (2), 1700157.

Hernández-Varela, J.D., Chanona-Pérez, J.J., Benavides, H.A.C., Sodi, F.C., Vicente-Flores, M., 2021. Effect of ball milling on cellulose nanoparticles structure obtained from garlic and agave waste. Carbohydr. Polym. 255, 117347.

Kalathil, S., Pant, D., 2016. Nanotechnology to rescue bacterial bidirectional extracellular electron transfer in bioelectrochemical systems. RSC Adv. 6 (36), 30582–30597.

Kavitha, V., Geetha, V., Jacqueline, P.J., 2019. Production of biodiesel from dairy waste scum using eggshell waste. Process Saf. Environ. Prot. 125, 279–287.

Khan, A.F., Mehmood, M., Durrani, S.K., Ali, M.L., Rahim, N.A., 2015. Structural and optoelectronic properties of nanostructured TiO2 thin films with annealing. Mater. Sci. Semicond. Process. 29, 161–169.

Khan, A., Toufiq, A.M., Tariq, F., Khan, Y., Hussain, R., Akhtar, N., ur Rahman, S., 2019. Influence of Fe doping on the structural, optical and thermal properties of α-MnO2 nanowires. Mater. Res. Express 6 (6), 065043.

Khan, A., Hussain, R., Toufiq, A.M., Shah, A., Khan, B.A., Niaz, Z., ur Rahman, S., 2020. Fabrication of cryptomelane FexMn1-xO2 with enhanced antibacterial activity and specific heat capacity. Mater. Charact. 169, 110661.

Kim, K.J., Kim, Y.J., Kim, J.H., Park, M.S., 2011. The effects of surface modification on carbon felt electrodes for use in vanadium redox flow batteries. Mater. Chem. Phys. 131 (1–2), 547–553.

Kim, B., Mohan, S.V., Fapyane, D., Chang, I.S., 2020. Controlling voltage reversal in microbial fuel cells. Trends Biotechnol. 38 (6), 667–678.

Krivenko, P.V., 1994. Alkaline cements. In: Proceedings of the 1st International Conference on Alkaline Cements And Concretes, Kiev, Ukraine, Vol. 1. VIPOL Stock Company, pp. 11–129.

Kumar, P.S., Ramya, C., Jayakumar, R., Lakshmanan, V.K., 2013. Drug delivery and tissue engineering applications of biocompatible pectin–chitin/nano CaCO3 composite scaffolds. Colloids Surf. B: Biointerfaces 106, 109–116.

Ławińska, K., Modrzewski, R., Obraniak, A., 2020. Comparison of granulation methods for tannery shavings. Fibres Text. East. Eur 28, 119–123.

Lee, K.R., Lee, J.H., Yoo, H.I., 2014. Grain size effect on the electrical properties of nanocrystalline ceria. J. Eur. Ceram. Soc. 34 (10), 2363–2370.

Li, C., Sun, H., Li, L., 2010. A review: the comparison between alkali-activated slag (Si+ Ca) and metakaolin (Si+ Al) cements. Cem. Concr. Res. 40 (9), 1341–1349.

Li, Z., Zhang, L., Amirkhiz, B.S., Tan, X., Xu, Z., Wang, H., Mitlin, D., 2012. Carbonized chicken eggshell membranes with 3D architectures as high-performance electrode materials for supercapacitors. Adv. Energy Mater. 2 (4), 431–437.

Liu, X., Yuan, F., Wei, Y., 2013. Grain size effect on the hardness of nanocrystal measured by the nanosize indenter. Appl. Surf. Sci. 279, 159–166.

Liu, F., Sun, L., Wan, J., Tang, A., Deng, M., Wu, R., 2019. Organic matter and ammonia removal by a novel integrated process of constructed wetland and microbial fuel cells. RSC Adv. 9 (10), 5384–5393.

Logan, B.E., 2008. Microbial Fuel Cells. John Wiley & Sons.

Lu, M., Qian, Y., Huang, L., Xie, X., Huang, W., 2015. Improving the performance of microbial fuel cells through anode manipulation. ChemPlusChem 80 (8), 1216–1225.

Ma, C.Y., Hou, C.H., 2019. Enhancing the water desalination and electricity generation of a microbial desalination cell with a three-dimensional macroporous carbon nanotube-chitosan sponge anode. Sci. Total Environ. 675, 41–50.
Mahmoud, M., Gad-Allah, T.A., El-Khatib, K.M., El-Gohary, F., 2011. Power generation using spinel manganese–cobalt oxide as a cathode catalyst for microbial fuel cell applications. Bioresour. Technol. 102 (22), 10459–10464.
Maltsev, A.A., Bibikov, S.B., Kalinichenko, V.N., Gudkov, M.V., Melnikov, V.P., Varfolomeev, S.D., 2018. Determining the specific surface area of carbon electrode materials for electrodes of supercapacitors via the adsorption of methylene blue dye. Russ. J. Phys. Chem. A 92 (4), 772–777.
Mathews, N.R., Morales, E.R., 2009. MA Corte's-Jacome, JA Toledo Antonio. Sol. Energy 83, 1499.
Mechiakh, R., Sedrine, N.B., Chtourou, R., Bensaha, R., 2010. Correlation between microstructure and optical properties of nano-crystalline TiO2 thin films prepared by sol–gel dip coating. Appl. Surf. Sci. 257 (3), 670–676.
Minakshi, M., Visbal, H., Mitchell, D.R., Fichtner, M., 2018. Bio-waste chicken eggshells to store energy. Dalton Trans. 47 (47), 16828–16834.
Minakshi, M., Higley, S., Baur, C., Mitchell, D.R., Jones, R.T., Fichtner, M., 2019. Calcined chicken eggshell electrode for battery and supercapacitor applications. RSC Adv. 9 (46), 26981–26995.
Mir, S.A., Gupta, D.C., 2019. Understanding the origin of half-metallicity and thermophysical properties of ductile La2CuMnO6 double perovskite. Int. J. Energy Res. 43 (9), 4783–4796.
Mudakkar, S.R., Zaman, K., Khan, M.M., Ahmad, M., 2013. Energy for economic growth, industrialization, environment and natural resources: living with just enough. Renew. Sust. Energ. Rev. 25, 580–595.
Murakami, F.S., Rodrigues, P.O., Campos, C.M.T.D., Silva, M.A.S., 2007. Physicochemical study of CaCO3 from egg shells. Food Sci.Technol. 27, 658–662.
Mustakeem, M., 2015. In: Electrode materials for microbial fuel cells: nanomaterial approach, 4, p. 22.
Nair, P.B., Justinvictor, V.B., Daniel, G.P., Joy, K., Ramakrishnan, V., Thomas, P.V., 2011. Effect of RF power and sputtering pressure on the structural and optical properties of TiO2 thin films prepared by RF magnetron sputtering. Appl. Surf. Sci. 257 (24), 10869–10875.
Nandiyanto, A.B.D., Oktiani, R., Ragadhita, R., 2019. How to read and interpret FTIR spectroscope of organic material. Indones.J.Sci.Technol. 4 (1), 97–118.
Offei, F., Thygesen, A., Mensah, M., Tabbicca, K., Fernando, D., Petrushina, I., Daniel, G., 2016. A viable electrode material for use in microbial fuel cells for tropical regions. Energies 9 (1), 35.
Owuamanam, S., Cree, D., 2020. Progress of bio-calcium carbonate waste eggshell and seashell fillers in polymer composites: a review. J.Compos.Sci. 4 (2), 70.
Palomo, A., Alonso, S., Fernandez-Jiménez, A., Sobrados, I., Sanz, J., 2004. Alkaline activation of fly ashes: NMR study of the reaction products. J. Am. Ceram. Soc. 87 (6), 1141–1145.
Peera, S.G., Maiyalagan, T., Liu, C., Ashmath, S., Lee, T.G., Jiang, Z., Mao, S., 2021. A review on carbon and non-precious metal based cathode catalysts in microbial fuel cells. Int. J. Hydrog. Energy 46 (4), 3056–3089.
Pérez-Rodríguez, P., Ovando-Medina, V.M., Martínez-Amador, S.Y., Rodríguez-de la Garza, J.A., 2016. Bioanode of polyurethane/graphite/polypyrrole composite in microbial fuel cells. Biotechnol. Bioprocess Eng. 21 (2), 305–313.
Pezoti, O., Cazetta, A.L., Bedin, K.C., Souza, L.S., Martins, A.C., Silva, T.L., Almeida, V.C., 2016. NaOH-activated carbon of high surface area produced from guava seeds as a high-efficiency adsorbent for amoxicillin removal: Kinetic, isotherm and thermodynamic studies. Chem. Eng. J. 288, 778–788.
Pisciotta, J.M., Zaybak, Z., Call, D.F., Nam, J.Y., Logan, B.E., 2012. Enrichment of microbial electrolysis cell biocathodes from sediment microbial fuel cell bioanodes. Appl. Environ. Microbiol. 78 (15), 5212–5219.
Rahimnejad, M., Adhami, A., Darvari, S., Zirepour, A., Oh, S.E., 2015. Microbial fuel cell as new technology for bioelectricity generation: a review. Alex.Eng.J. 54 (3), 745–756.
Sami, S.K., Seo, J.Y., Hyeon, S.E., Shershah, M.S.A., Yoo, P.J., Chung, C.H., 2018. Enhanced capacitive deionization performance by an rGO–SnO 2 nanocomposite modified carbon felt electrode. RSC Adv. 8 (8), 4182–4190.
Sravan, J.S., Raunija, T.S.K., Verma, A., Mohan, S.V., 2021. Impregnated thermoset pre-pressurized carbon composite electrodes in microbial fuel cell: compositional functionalities influence on ORR with reference to graphite. Fuel 285, 119273.
Tsai, W.T., Yang, J.M., Lai, C.W., Cheng, Y.H., Lin, C.C., Yeh, C.W., 2006. Characterization and adsorption properties of eggshells and eggshell membrane. Bioresour. Technol. 97 (3), 488–493.
Tseng, T.M., Huang, R.H., Huang, C.Y., Liu, C.C., Hsueh, K.L., Shieu, F.S., 2014. Carbon felt coated with titanium dioxide/carbon black composite as negative electrode for vanadium redox flow battery. J. Electrochem. Soc. 161 (6), A1132.
Williams, R.A., LeBlanc, L.J., Jimenez-Garcia, K., Beeler, M.C., Perry, A.R., Phillips, W. D., Spielman, I.B., 2012. Synthetic partial waves in ultracold atomic collisions. Science 335 (6066), 314–317.
Xi, Y., Gao, K., Pang, X., Yang, H., Xiong, X., Li, H., Volinsky, A.A., 2017. Film thickness effect on texture and residual stress sign transition in sputtered TiN thin films. Ceram. Int. 43 (15), 11992–11997.
Xiong, J., Das, S.N., Kim, S., Lim, J., Choi, H., Myoung, J.M., 2010. Photo-induced hydrophilic properties of reactive RF magnetron sputtered TiO2 thin films. Surf. Coat. Technol. 204 (21–22), 3436–3442.
Xu, A.W., Yu, Q., Dong, W.F., Antonietti, M., Cölfen, H., 2005. Stable amorphous CaCO3 microparticles with hollow spherical superstructures stabilized by phytic acid. Adv. Mater. 17 (18), 2217–2221.
Yaqoob, A.A., Ibrahim, M.N.M., Yaakop, A.S., 2021. Application of oil palm lignocellulosic derived material as an efficient anode to boost the toxic metal remediation trend and energy generation through microbial fuel cells. J. Clean. Prod. 314, 128062.
Yaqoob, A.A., Al-Zaqri, N., Yaakop, A.S., Umar, K., 2022. Potato waste as an effective source of electron generation and bioremediation of pollutant through benthic microbial fuel cell. Sustain.Energy Technol.Assess. 53, 102560.
Zhao, Y., Zhang, X., Chen, X., Li, W., Wang, L., Ren, F., Li, Y., 2020. Preparation of WO3 films with controllable crystallinity for improved near-infrared electrochromic performances. ACS Sustain. Chem. Eng. 8 (31), 11658–11666.
Zhou, H., Zhang, H., Zhao, P., Yi, B., 2006. A comparative study of carbon felt and activated carbon based electrodes for sodium polysulfide/bromine redox flow battery. Electrochim. Acta 51 (28), 6304–6312.

Effect of NaOH concentration as activator on calcined eggshell and its application for yeast microbial fuel cell

ORIGINALITY REPORT

16%	11%	13%	4%
SIMILARITY INDEX	INTERNET SOURCES	PUBLICATIONS	STUDENT PAPERS

PRIMARY SOURCES

1	repository.iti.ac.id Internet Source	2%
2	Mohamed Mahmoud, K.M. El-Khatib. "Three-dimensional graphitic mesoporous carbon-doped carbon felt bioanodes enables high electric current production in microbial fuel cells", International Journal of Hydrogen Energy, 2020 Publication	1%
3	www.alice.cnptia.embrapa.br Internet Source	1%
4	Submitted to The University of Manchester Student Paper	1%
5	link.springer.com Internet Source	<1%
6	Submitted to CSU, Fullerton Student Paper	<1%
7	www.mdpi.com Internet Source	<1%

8	Marcelinus Christwardana, J. Joelianingsih, Linda Aliffia Yoshi, H. Hadiyanto. "Binderless carbon nanotube/carbon felt anode to improve yeast microbial fuel cell performance", Current Research in Green and Sustainable Chemistry, 2022 Publication	<1 %
9	Mohammed Al-Sahari, Adel Al-Gheethi, Radin Mohamed, Efaq Noman, M. Naushad, Mohd Baharudin Rizuan, Dai-Viet N. Vo, Norli Ismail. "Green approach and strategies for wastewater treatment using bioelectrochemical systems: A critical review of fundamental concepts, applications, mechanism, and future trends", Chemosphere, 2021 Publication	<1 %
10	Zhang, J.. "Preparation and characterization of sol-gel Al-doped ZnO thin films and ZnO nanowire arrays grown on Al-doped ZnO seed layer by hydrothermal method", Solar Energy Materials and Solar Cells, 201012 Publication	<1 %
11	moam.info Internet Source	<1 %
12	www.investigo.biblioteca.uvigo.es Internet Source	<1 %

13	"Microbial Fuel Cell", Springer Science and Business Media LLC, 2018 Publication	<1 %
14	ndl.ethernet.edu.et Internet Source	<1 %
15	"Handbook of Ecomaterials", Springer Nature, 2019 Publication	<1 %
16	Chengyu Wang, Yang Xu, Yalan Liu, Jian Li. "Synthesis and characterization of lamellar aragonite with hydrophobic property", Materials Science and Engineering: C, 2009 Publication	<1 %
17	I. Garcia-Lodeiro, A. Palomo, A. Fernández-Jiménez. "An overview of the chemistry of alkali-activated cement-based binders", Elsevier BV, 2015 Publication	<1 %
18	aip.scitation.org Internet Source	<1 %
19	dokumen.pub Internet Source	<1 %
20	mdpi-res.com Internet Source	<1 %
21	media.neliti.com Internet Source	<1 %

22	repositorium.sdum.uminho.pt Internet Source	<1 %
23	worldwidescience.org Internet Source	<1 %
24	Min Chan Kim, Sang Yun Kim, Kwan Woo Kim. "Laparoscopic Reinforcement Suture (LARS) on Staple Line of Duodenal Stump Using Barbed Suture in Laparoscopic Gastrectomy for Gastric Cancer: a Prospective Single Arm Phase II Study", Journal of Gastric Cancer, 2017 Publication	<1 %
25	daneshyari.com Internet Source	<1 %
26	Alena Opálková Šišková, Tomáš Dvorák, Tímea Šimonová Baranyaiová, Erik Šimon et al. "Simple and Eco-Friendly Route from Agro-Food Waste to Water Pollutants Removal", Materials, 2020 Publication	<1 %
27	ejournal.undip.ac.id Internet Source	<1 %
28	library.unisel.edu.my Internet Source	<1 %
29	Submitted to Loughborough University Student Paper	<1 %

30	Marcelinus Christwardana, J. Joelianingsih, Linda Aliffia Yoshi. "A novel of 2D-3D combination carbon electrode to improve yeast microbial fuel cell performance", Journal of Applied Electrochemistry, 2022 Publication	<1 %
31	Miriam Rosenbaum, Feng Zhao, Uwe Schröder, Fritz Scholz. "Interfacing Electrocatalysis and Biocatalysis with Tungsten Carbide: A High-Performance, Noble-Metal-Free Microbial Fuel Cell", Angewandte Chemie, 2006 Publication	<1 %
32	dspace01.jaist.ac.jp Internet Source	<1 %
33	globaleducationforum.org Internet Source	<1 %
34	"Bioelectrochemical Interface Engineering", Wiley, 2019 Publication	<1 %
35	"Bioelectrochemical Systems", Springer Science and Business Media LLC, 2020 Publication	<1 %
36	Thi Xuan Huong Le, Mikhael Bechelany, Marc Cretin. "Carbon felt based-electrodes for energy and environmental applications: A review", Carbon, 2017	<1 %

	Publication	
37	downloads.hindawi.com Internet Source	<1 %
38	infid.org Internet Source	<1 %
39	scholar.sun.ac.za Internet Source	<1 %
40	www.nature.com Internet Source	<1 %
41	Indrasis Das, Md. T. Noori, Melad Shaikh, Makarand M. Ghangrekar, Rajakumar Ananthakrishnan. "Synthesis and Application of Zirconium Metal–Organic Framework in Microbial Fuel Cells as a Cost-Effective Oxygen Reduction Catalyst with Competitive Performance", ACS Applied Energy Materials, 2020 Publication	<1 %
42	garuda.kemdikbud.go.id Internet Source	<1 %
43	li.mit.edu Internet Source	<1 %
44	"Emerging Nanomaterials for Advanced Technologies", Springer Science and Business Media LLC, 2022 Publication	<1 %

45	Wang, Huanlei, Zhi Li, Jin Kwon Tak, Chris M.B. Holt, Xuehai Tan, Zhanwei Xu, Babak Shalchi Amirkhiz, Don Harfield, Anthony Anyia, Tyler Stephenson, and David Mitlin. "Supercapacitors based on carbons with tuned porosity derived from paper pulp mill sludge biowaste", Carbon, 2013. Publication	<1 %
46	diglib.tugraz.at Internet Source	<1 %
47	dspace.nm-aist.ac.tz Internet Source	<1 %
48	www.cityofevanston.org Internet Source	<1 %
49	Azman, Nadia Farhana, Peyman Abdeshahian, Abudukeremu Kadier, Hafiza Shukor, Najeeb Kaid Nasser Al-Shorgani, Aidil Abdul Hamid, and Mohd Sahaid Kalil. "Utilization of palm kernel cake as a renewable feedstock for fermentative hydrogen production", Renewable Energy, 2016. Publication	<1 %
50	Farhan Papiya, Prasanta Pattanayak, Piyush Kumar, Vikash Kumar, Patit Paban Kundu. "Development of highly efficient bimetallic nanocomposite cathode catalyst, composed of Ni:Co supported sulfonated polyaniline for	<1 %

application in microbial fuel cells", Electrochimica Acta, 2018
Publication

---

51 Green Energy and Technology, 2015. <1%
Publication

---

52 H. Hadiyanto, Marcelinus Christwardana, W. Widayat, Andono Kusuma Jati, Salsabella Indy Laes. "Optimization of flocculation efficiency and settling time using chitosan and eggshell as bio-flocculant in Chlorella pyrenoidosa harvesting process", Environmental Technology & Innovation, 2021 <1%
Publication

---

53 H. Hadiyanto, Marcelinus Christwardana, Wahyu Zuli Pratiwi, P. Purwanto, S. Sudarno, Kristinah Haryani, Anh Tuan Hoang. "Response surface optimization of microalgae microbial fuel cell (MMFC) enhanced by yeast immobilization for bioelectricity production", Chemosphere, 2022 <1%
Publication

---

54 Sharma, S.D.. "Sol-gel-derived super-hydrophilic nickel doped TiO"2 film as active photo-catalyst", Applied Catalysis A, General, 20061025 <1%
Publication

---

55 Yi-Xuan Wang, Wen-Qiang Li, Chuan-Shu He, Guan-Nan Zhou, Hou-Yun Yang, Jun-Cheng <1%

Han, Shi-Qi Huang, Yang Mu. "Efficient bioanode from poultry feather wastes-derived N-doped activated carbon: Performance and mechanisms", Journal of Cleaner Production, 2020
Publication

---

56 Yong Yuan, Shungui Zhou, Yi Liu, Jiahuan Tang. "Nanostructured Macroporous Bioanode Based on Polyaniline-Modified Natural Loofah Sponge for High-Performance Microbial Fuel Cells", Environmental Science & Technology, 2013 <1%
Publication

---

57 Zafar Ali, Javaid Ismail, Rafaqat Hussain, A. Shah, Arshad Mahmood, Arbab Mohammad Toufiq, Shams ur Rahman. " Hydrothermal synthesis and characterization of carbon-doped TiO nanoparticles ", Chinese Physics B, 2020 <1%
Publication

---

58 neuroquantology.com <1%
Internet Source

---

59 orca.cf.ac.uk <1%
Internet Source

---

60 scholarbank.nus.edu.sg <1%
Internet Source

---

61 studentsrepo.um.edu.my
Internet Source

		<1%
62	trepo.tuni.fi Internet Source	<1%
63	"Chemically Deposited Nanocrystalline Metal Oxide Thin Films", Springer Science and Business Media LLC, 2021 Publication	<1%
64	Atefeh Taherniya, Davood Raoufi. " The annealing temperature dependence of anatase TiO thin films prepared by the electron-beam evaporation method ", Semiconductor Science and Technology, 2016 Publication	<1%
65	Junhong Chen, Yadong Mei. "Ecological Network Analysis of a Virtual Water System in Tibet, China", Water, 2021 Publication	<1%
66	Marcelinus Christwardana, Aniek Sri Handayani, Rike Yudianti, Joelianingsih. "Cellulose – Carrageenan coated carbon felt as potential anode structure for yeast microbial fuel cell", International Journal of Hydrogen Energy, 2020 Publication	<1%

Exclude quotes	Off	Exclude matches	Off
Exclude bibliography	On		

Effect of NaOH concentration as activator on calcined eggshell and its application for yeast microbial fuel cell

GRADEMARK REPORT

FINAL GRADE

/0

GENERAL COMMENTS

Instructor

PAGE 1

PAGE 2

PAGE 3

PAGE 4

PAGE 5

PAGE 6

PAGE 7

PAGE 8

PAGE 9

PAGE 10

PAGE 11